PASJ: Publ. Astron. Soc. Japan **51**, 737–743 (1999)

Central Kinematics and Rotation Curve of the Sb Galaxy NGC 4527 in CO, Hα, and [N II] Lines

Yoshiaki SOFUE,[1] Akihiko TOMITA,[2] Mareki HONMA,[1,3] and Yoshinori TUTUI[1]

1 Institute of Astronomy, The University of Tokyo, Mitaka, Tokyo 181-8588
2 Faculty of Education, Wakayama University, Wakayama 640-8510
3 National Astronomical Observatory, Mitaka, Tokyo 181-8588

(Received 1998 March 23; accepted 1999 August 26)

Abstract

We have obtained interferometer observations of the central region of the Sb galaxy NGC 4527 in the CO (J = 1–0) line emission using the Nobeyama Millimeter Array. We also obtained optical (Hα, [N II]) spectroscopy using the Okayama 188-cm reflector along the major axis. The kinematical structure and the distribution of H II regions show symmetry around the nucleus, while the distribution of molecular gas is asymmetric. The molecular-gas mass shares only 10% of the dynamical mass in the central 1 kpc radius region. Using position–velocity diagrams, we have derived a center-to-disk rotation curve. It rises steeply in the central region, attaining a maximum of about 250 km s^{-1} at 400 pc radius, and then decreases to a minimum at 2 kpc radius, followed by a disk and outer flat part. The rotation curve may provide us with the most similar case to that of the Milky Way Galaxy.

Key words: Galaxies: general — Galaxies: kinematics — Galaxies: molecular gas — Galaxies: rotation

1. Introduction

CO line emission can be an ideal tool to derive rotation curves in the central regions of galaxies (Sofue 1996, 1997; Sofue et al. 1997, 1998, 1999), because the CO gas is concentrated in the inner few kpc region (Sofue et al. 1994). Since the CO gas coexists with H II regions, Hα-line spectroscopy will also be useful to derive rotation curves at the central region, if the bulge light can be subtracted and the extinction is small enough. In fact, Rubin et al. (1997) have obtained extensive Hα spectroscopy for Virgo spirals, and have shown a steep rise of the rotation curves at the central regions for many galaxies. On the other hand, outer rotation and kinematics have been investigated based on optical and H I line observations (Rubin et al. 1980, 1982; Bosma 1981; Mathewson, Ford 1996; Persic, Salucci 1995; Persic et al. 1996).

In order to derive detailed central rotation curves of galaxies, we have performed CO and Hα line spectroscopy for many galaxies using high-resolution CO-line observations as well as in the Hα and [N II] lines. In this paper, we present the result for the Sb galaxy NGC 4527 (table 1), which is one of the CO-rich galaxies with a high molecular-gas concentration near the center (Young et al. 1995) and having a weak star-burst activity (Soifer et al. 1987).

2. Observations

2.1. CO Observations

High-resolution interferometer observations were obtained by using the Nobeyama Millimeter Array (NMA) in the C configuration on 1994 December 2 and in the D configuration on 1995 March 16. Flux and phase calibrations were performed by observing the nearby radio source 3C 273, which had a flux density of 22 Jy at the observing frequency. A 1024-channel FX system (a fast-Fourier-transform spectro-correlator) was used for spectroscopic data acquisition with a total bandwidth of 320 MHz (831 km s^{-1}). The data were then averaged in 16 bins of the original frequency channels, resulting in 64 channels with a frequency (velocity) resolution of 5 MHz (13.0 km s^{-1}). The cleaned maps were then combined into a cube of intensity data in the (RA, Dec, $V_{\rm LSR}$) space. Using the data cube, we obtained an intensity map, velocity field map, and position–velocity diagrams along the major axis. The synthesized beam was $9\farcs52 \times 5\farcs61$, which yielded a brightness temperature-to-flux density ratio of 1.725 K/(Jy/beam). The observational parameters are summarized in table 1.

2.2. Optical Spectroscopy

CCD optical observations were made using a Cassegrain spectrometer equipped on a 188-cm reflector at the Okayama Astrophysical Observatory. The slit

Table 1. Observed parameters for NGC 4527.

Type	Sb(c)
NED position (1950)	RA = $12^h31^m35^s.4$
	Dec = 02°55′43″
CO kinematical center (1950)	RA = $12^h31^m34^s.9$
	Dec = 02°55′45″
Apparent magnitude† B_T	11.32
Corrected Apparent magnitude $B_T^{0,i}$	10.30
Systemic recession velocity, V_{sys}	1750 km s^{-1}
Assumed distance, D	22 Mpc (H_0 = 75 km s^{-1} Mpc^{-1})
	(10″ = 1.05 kpc)
Optical inclination angle i	69°
Optical position angle	66°
CO position angle	80°
CO kinematical position angle	55°
CO peak intensity, $I_{co,peak}$	112 Jy/beam km s^{-1} = 193 K km s^{-1}
CO luminosity, L_{CO}	3.65(±0.54) × 10^8 K km s^{-1} pc^2
Molecular hydrogen mass, M_{H_2}	5.31(±0.78) × 10^8 $M_\odot$
Molecular gas mass, $M_{mol.gas}$	8.72(±1.28) × 10^8 $M_\odot$ (X = 0.61)
Dynamical mass within 1 kpc (10″) radius	7.5 × 10^9 $M_\odot$
Far-IR luminosity‡, L_{FIR}(42.5–122.5 μm)	7.4 × 10^{10} $L_\odot$
CO velocity width, $W_{CO}^{0,i}$	452 km s^{-1}
Hα velocity width, $W_{H_\alpha}^{0,i}$	451 km s^{-1}

†Sandage, Tamman (1981); ‡Soifer et al. (1987).

width was 1.″9, which was similar to the seeing size, and was put crossing the nucleus at a position angle of 66°. The CCD chip had 512 × 512 pixels; we have averaged values in every 2 pixels in spatial direction to increase the signal-to-noise ratio, resulting in 1.″5 per pixel, and the spectral dispersion was 0.767 Å (velocity spacing of 34.9 km s^{-1}) per pixel. Taking into account the seeing size, pixel binding, and the tracking error during observations, we estimate the spatial resolution to be about 3″. Taking into account the slit width, the effective spectral resolution was 1.92 Å, which corresponds to a velocity resolution of 87.1 km s^{-1}. We finally used 160 pixels (4′) in the spatial direction, and 270 pixels of wavelength range of 207 Å including the Hα and [N II] line emissions. The exposure time was 1000 s per one spectrum, and we took three spectra for the galaxy and combined them.

The continuum emission, such as that due to the bulge, has been subtracted by applying a background-filtering technique (Sofue, Reich 1979). We first smoothed the original spectrum S_0 in the wavelength direction by a convolution function of width $\Delta x \times \Delta\lambda = 1 \times 100$, where x is the position in pixel along the major axis and λ the pixels in the wavelength direction. The convoluted spectrum S_1 was subtracted from the original to get $S_2 = S_0 - S_1$. The negative values in S_2 was replaced with 0, and S_2 is subtracted from the original to get $S_3 = S_0 - S_2$. We smooth S_3 by the same convolution function, and obtained S_4. Then, we replaced S_1 with S_4, and applied again the above procedure, and repeated this procedure for several times. We finally obtained a 'background (continuum)'-subtracted spectrum, $S_{cont.free} = S_0 - S_1(i\text{-th})$. The spurious lines from the atmosphere, which are at the rest wavelengths, are also subtracted from the spectrum.

3. Results

3.1. CO-Intensity Distribution and Molecular Gas Mass

Figure 1 summarizes the observed results, as superposed on the DSS B-band image of NGC 4527. Figure 2 shows the obtained distribution of the integrated CO-line intensity. The molecular-gas distribution is elongated in the direction of the position angle of 80°, about 14° shifted from the major axis of the galaxy. The gas distribution comprises two large clumps, and is highly asymmetric with respect to the center: the western clump is much brighter than the eastern one. The peak intensity of $I_{co,peak}$ = 112 Jy/beam km s^{-1} = 193 K km s^{-1} is obtained at RA = $12^h31^m34^s.52$, Dec=02°55′45.″0. An arm-like feature is extending toward the east from the eastern clump, coinciding with an optical spiral arm. A counter part to this arm appears to be present in the western side.

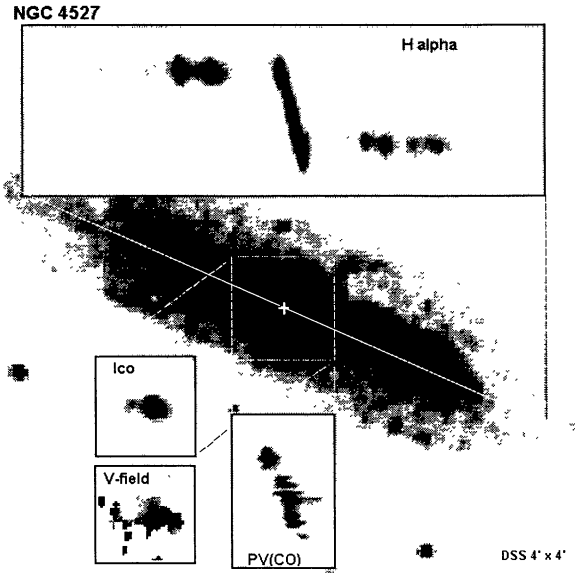

Fig. 1. Observed results superposed on a DSS B-band image of NGC 4527.

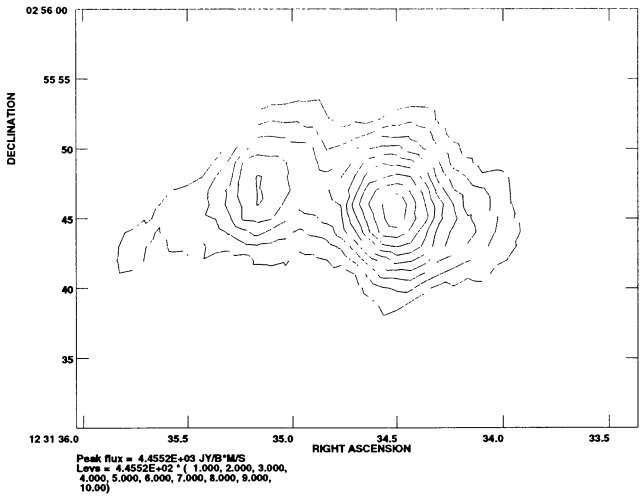

Fig. 2. CO ($J = 1$–0) line intensity map as obtained by Nobeyama Millimeter Array. The contours are every 10% of the peak intensity (= 169 K km s^{-1}).

The total CO luminosity integrated within $40'' \times 30''$ area centered on the map center is estimated to be $L_{\rm co} = 3.65(\pm 0.54) \times 10^8$ K km s^{-1} pc^2 for an assumed distance of $D = 22$ Mpc. This yields a mass of molecular hydrogen gas of $M_{\rm H_2} = CL_{\rm co} = 5.31(\pm 0.78) \times 10^8\, M_\odot$; the total mass of molecular gas is given by $M_{\rm mol.gas} = M_{\rm H_2}/X = 8.72(\pm 1.28) \times 10^8 M_\odot$ for $X = 0.61$. Here, the correction factor X from the hydrogen mass to real gas mass, including He and heavier elements, was taken from Sofue (1995) for the Milky Way Center, and the conversion factor at the center of a galaxy, $C = 0.92 \times 10^{20}$ H$_2$ /(K km s^{-1}), was taken from Arimoto et al. (1996).

The dynamical mass $M_{\rm dyn}$ can be estimated from the rotation curve, as obtained in the next section. The dynamical mass within 1 kpc radius, where the major CO features are included, is estimated to be $\sim 7.5 \times 10^9\, M_\odot$, which yields a molecular mass fraction in total (dynamical) mass of about 0.12. The dynamical mass within the 1.5 kpc radius ($15''$) region, where the CO map is obtained, is $1.7 \times 10^{10}\, M_\odot$, yielding a molecular mass fraction of only 0.051. Therefore, the molecular-to-total mass ratio in the central region of NGC 4527 is not particularly high, but is approximately the same as that of the mean value in the whole Milky Way.

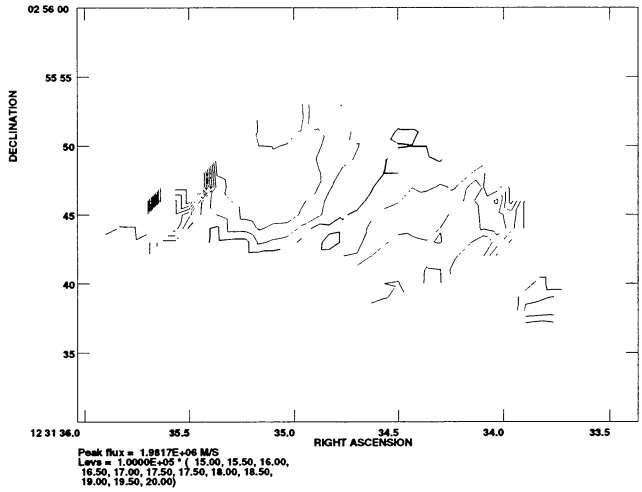

Fig. 3. Intensity-weighted mean velocity field (moment 1) of the CO line emission. Contours are drawn at velocity intervals of 50 km s^{-1}. The thick contour near the center is at 1750 km s^{-1}, and the velocity increases from right to left (blue-shifted in W side; red-shifted in E side).

3.2. CO Velocity Field

The distribution of the intensity-weighted mean velocity of the CO-line emission is shown in figure 3. Equal-velocity contours around the nucleus are aligned at a position angle of $-35°$, showing that the rotating disk has the major axis at 55°. This direction is shifted by about $j = 11°$ from that of the optical major axis of the galaxy (66°) in the opposite sense to that of the elongation of the intensity map. If we take into account the inclination of the galaxy, $i = 69°$, the tilt of the equal-velocity contours from a pure-circular velocity contours on the plane of the galaxy, j_0, is given by $\tan j_0 = \cos i \, \tan j$; there-

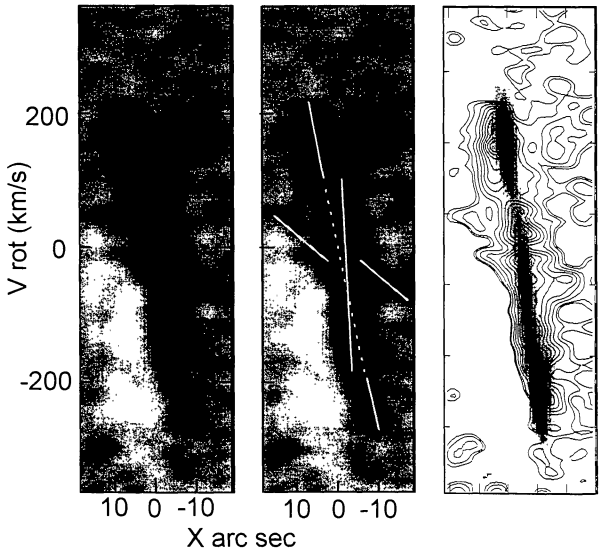

Fig. 4. Left panel: CO-line position–velocity diagram along the major axis of NGC 4527. The velocity is corrected for the inclination. Middle: The white lines in the middle panel indicate major PV features. Right panel: Hα line PV diagram is superposed in gray on the CO PV diagram in contours. The CO contours are every 10% of the peak temperature of 0.895 K.

fore, $j_0 = 4°$. Hence, non-circular velocities of the disk rotation is estimated to be $V_{\rm rot} \sin j_0 \sim 13$ km s^{-1}, of the order of the velocity resolution of CO observation. So, we may safely assume that the rotation of the CO disk is approximately circular.

3.3. *CO Position–Velocity Diagram*

Figure 4 shows the obtained position–velocity (PV) diagram of the CO line emission along the major axis. The major PV feature shows a peculiar bend, which can be interpreted as being due to two superposed PV features: (a) a steep component with a velocity gradient as large as 200 km s^{-1}/5″= 200 km s^{-1}/400 pc across the nucleus, which indicates a molecular disk or ring of radius 3″, or 240 pc. (b) a higher-velocity, larger-radius ring with a velocity gradient of 450 km s^{-1}/15″ = 225 km s^{-1}/7.5″ = 225 km s^{-1}/600 pc. In addition to these major features, we can recognize (c) a lower-velocity, smaller-gradient PV component crossing the major PV feature, which may be due to foreground/background spiral arms. This low-velocity component is also clearly visible in the optical PV diagrams in the Hα and [N II] lines (figure 5).

3.4. *Hα and [N II] Position–Velocity Diagrams*

Figure 5 shows the Hα (lower) and [N II] (upper) PV diagrams, where the continuum light has been subtracted by using the background-filtering technique. The rotation velocity in the Hα and [N II] emission lines rises very steeply near the nucleus. The Hα PV diagram shows a steep rise in the central region with a slope of 200 km s^{-1}/4″ =200 km s^{-1}/400 pc, also indicating a ring-like distribution of H II regions with a radius of 450 pc. This feature coincides with the innermost, steep velocity gradient CO feature. In the right panel of figure 4, we superpose the CO and Hα PV diagrams. It is interesting to note that the Hα feature is located inside the high-velocity CO feature (b).

The [N II] PV diagram shows about the same behavior as the Hα line. However, the innermost [N II] feature shows a higher-velocity component with a steeper gradient, which is more coincident with the innermost CO PV feature. This [N II] feature attains a maximum velocity of about 250 km s^{-1} in the central 400 pc region, indicating a very steep rise of the rotation curve in the inner 400 pc, attaining a maximum velocity as high as 250 km s^{-1}. Since the Hα line could be superposed by a broad Balmer absorption wing toward a star-forming a disk in a galaxy, the [N II] line would be more reliable to trace the innermost kinematics (see Sofue et al. 1997). Therefore, we adopt the largest rotation velocities for the innermost region, e.g., within 500 pc.

3.5. *Line Profiles*

Figure 6 shows line profiles of the CO, Hα, and [N II] lines. Note that the Hα and [N II] PV diagrams are similar to each other, indicating that the Hα line profile is not affected by the AGN activity. the CO profile is more complicated compared to the optical profiles, which may indicate a more irregular distribution of molecular gas compared to the star-forming regions, which is already revealed by the asymmetric CO-intensity distribution. Both the Hα and [N II] optical profiles are characterized by their double horn feature, typical for a rotating disk. The line widths for CO and Hα lines are, however, very similar, both about 450 km s^{-1} at the 20% level of the peak intensity, indicating that molecular gas and star-forming regions are rotating in a similar manner.

3.6. *CO Asymmetry vs Kinematical Symmetry*

Although the kinematical property is nearly symmetric as can be seen in the PV diagrams and velocity field, some small non-circular motion of ~ 13 km s^{-1} appears to be superposed, suggesting a slightly distorted potential and density waves. Since the gas mass is much smaller than the dynamical mass, such density waves would cause a non-linear response of the gas associated with strong compression, resulting in an asymmetry of the molecular gas distribution. Star formation would occur intensely in such compressed gaseous regions. In fact, NGC 4527 shows a weak starburst. The far-infrared luminosity is

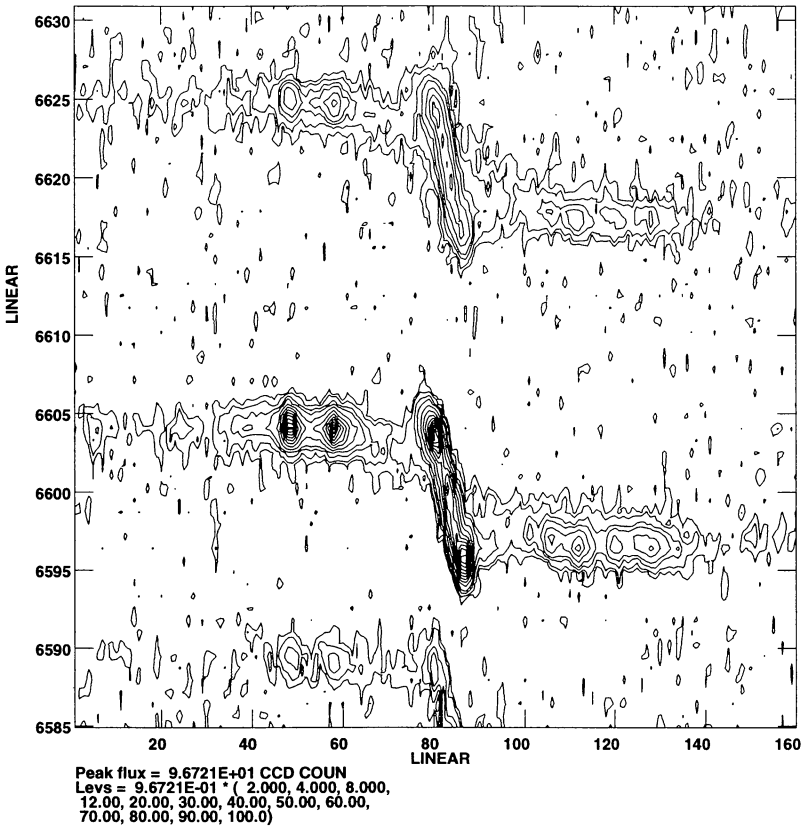

Fig. 5. Hα (lower) and [N II] (upper) position–velocity diagrams along the major axis of NGC 4527, as obtained with the Okayama 188-cm telescope. Continuum bulge emission has been subtracted. The indicated contour levels are in CCD counts after integrating all observed frames. The intensity scale is not calibrated because of the unknown extinction. Note higher velocities in the [N II] line for the innermost regions.

$L_{\rm FIR} = 7.4 \times 10^{10} L_{\odot}$ (Soifer et al. 1987) corresponding to a star-formation rate of $10\,M_{\odot}$ yr^{-1} (Sauvage, Thuan 1992), much more intense than that of our Galaxy center.

3.7. Rotation Curve

We derived a rotation curve by applying an envelope-tracing method (Sofue 1996) to the present PV diagrams. The velocity dispersion of the interstellar gas ($\sigma_{\rm ISM}$) and the velocity resolution of observations ($\sigma_{\rm obs}$) were corrected for as the following. The correction for the finite-velocity resolution, $\sigma_{\rm obs} = 0.5\,{\rm FWHM}$ (full width of half maximum), is given by

$$\sigma_{\rm cor} = \sigma_{\rm obs} \exp[-(d/\sigma_{\rm obs})^2]. \quad (1)$$

Here, d is the velocity difference between the maximum-intensity velocity near the profile edge, and the half-maximum velocity (half width of the intensity slope at the velocity edge). Equation (1) implies that, if the original velocity profile of the source is sharp enough, the observed profile becomes the telescope velocity profile, so that the correction is equal to the velocity resolution ($\sigma_{\rm cor} = \sigma_{\rm obs}$). On the other hand, if the velocity profile of the source is extended largely ($d \gg \sigma_{\rm obs}$), the correction becomes negligible ($\sigma_{\rm cor} \sim 0$) and the half-maximum velocity gives the rotation velocity.

The terminal velocity $V_{\rm t}$ is defined by the velocity at which the intensity becomes equal to $I_{\rm t} = 0.5 I_{\rm max}$ in the PV diagrams. Then, the rotation velocity is estimated by $V_{\rm rot} = [V_{\rm t} - (\sigma_{\rm cor}^2 + \sigma_{\rm ISM}^2)^{1/2}]/\sin i$. For the present galaxy, we take $\sigma_{\rm ISM} \sim 7$ km s^{-1}, $\sigma_{\rm obs} = 13/2 = 6.5$ km s^{-1} for CO, and $\sigma_{\rm obs} = 87/2 = 43.5$ km s^{-1} for Hα.

The obtained rotation curve using the CO, Hα, and [N II] PV data is shown in figure 7. The innermost curve within 500 pc radius was obtained by adopting the largest values among the three lines, because the CO data may miss the highest velocities for its lower angular resolution than optical. The curve at radius 500 to 1.5 kpc is an average of the three lines, and the outer part is based on the Hα line alone. The CO and Hα rotation curves derived by this method show a maximum of 250 km s^{-1} in

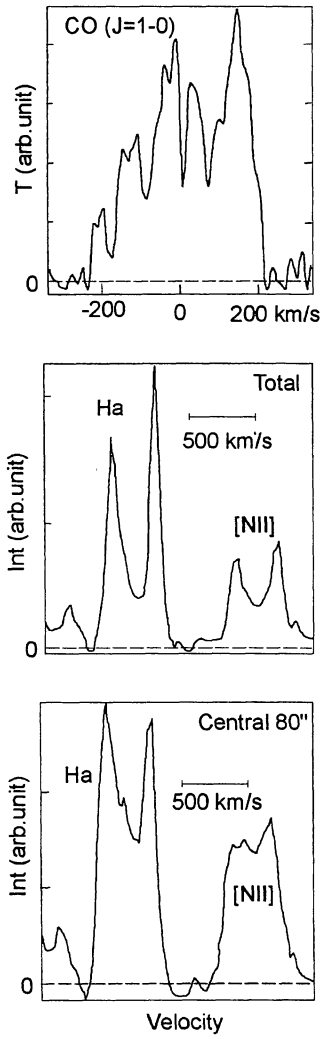

Fig. 6. Line profiles of the CO line (top), Hα and [N II] lines averaged along the whole major axis (middle), and the same for the central 80″ region (bottom).

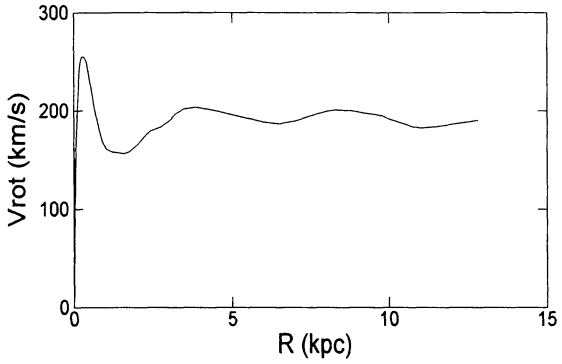

Fig. 7. Rotation curve of NGC 4527, as obtained from the observed PV diagrams in the CO, Hα, and [N II] lines.

the 500-pc ring. The rotation velocity, then, decreases to 170 km s^{-1} at 2 kpc, beyond which, it increases gradually to attain a flat rotation of about 200 km s^{-1} at radius 5 to 12 kpc. The combined rotation curve from the CO and Hα data is shown by the thick line in the figure.

The high-velocity rotation around the center may indicate the existence of a massive core with a scale radius smaller than several times 100 pc, possibly in addition to the bulge component obeying an exponential or a de Vaucouleurs law. The rotation curve of NGC 4527 shows a remarkable similarity to the rotation curve of the Milky Way and many other galaxies. We stress that such a behavior of nuclear rise of rotation curves will be universal for massive spiral galaxies, with only a few exceptions of dwarf and small-mass galaxies (Sofue et al. 1997).

4. Discussion

We have obtained interferometer observations of the CO ($J = 1$–0) line emission using the Nobeyama Millimeter Array, and Hα and [N II] line spectroscopy using the Okayama 188-cm reflector along the major axis. While the CO distribution shows asymmetry and is elongated in a direction at a position angle of 80°, the kinematical position angle inferred from the velocity field is 55° and approximately coincides with the direction of the optical major axis, suggesting that the non-circular motion is not dominant. Besides the kinematical structure, the distribution of H II regions in the PV diagram show symmetry around the nucleus. The molecular-gas mass inferred from the CO intensity shares only 10% of the total (dynamical) mass in the central 1 kpc radius region, and is only 5% in 1.5 kpc radius region.

We have derived a nucleus-to-disk rotation curve using the CO, Hα, and [N II] PV diagrams along the major axis. The rotation velocity rises steeply within 400 pc of the nucleus to about 230–250 km s^{-1}, indicating a massive core around the nucleus. The rotation curve, then, decreases to a minimum at 2 kpc, followed by a disk and outer flat part. Such a behavior of the rotation curve mimics that of the Galaxy and of many other galaxies.

The observations were made during a course of common-use programs at the Nobeyama Radio Observatory and the Okayama Astrophysical Observatory of the National Astronomical Observatories. The authors thank the staff of the observatories for their help and invaluable suggestions during the observations.

References

Arimoto N., Sofue Y., Tsujimoto T. 1996, PASJ 48, 275
Bosma A. 1981, AJ 86, 1825
Mathewson D.S., Ford V.L. 1996, ApJS 107, 97
Persic M., Salucci P. 1995, ApJS 99, 501
Persic M., Salucci P., Stel F. 1996, MNRAS 281, 27
Rubin V.C., Ford W.K. Jr, Thonnard N. 1980, ApJ 238, 471
Rubin V.C., Ford W.K. Jr, Thonnard N. 1982, ApJ 261, 439
Rubin V.C., Kenney J.D.P., Young J.S. 1997, AJ 113, 1250
Sandage A., Tammann G.A. 1981, in A Revised Shapley-Ames Catalog of Bright Galaxies, Carnegie Institution of Washigton Pubication 635 (Washington D.C.)
Sauvage M., Thuan T. 1992, ApJ 396, L69
Sofue Y. 1995, PASJ 47, 527
Sofue Y. 1996, ApJ 458, 120
Sofue Y. 1997, PASJ 49, 17
Sofue Y., Honma M., Arimoto N. 1994, A&A 296, 33
Sofue Y., Honma M., Tutui Y., Tomita A. 1997, AJ 114, 2428
Sofue Y., Reich W. 1979, A&A 38, 251
Sofue Y., Tomita A., Honma M., Tutui Y., Takeda Y. 1998, PASJ 50, 427
Sofue Y., Tutui Y., Honma M., Tomita A., Takamiya T., Koda J., Takeda Y. 1999, ApJ in press
Soifer B.T., Sanders D.B., Madore B.F., Neugebauer G., Danielson G.E., Elias J.H., Lonsdale C.J., Rice W.L. 1987, ApJ 320, 238
Young J.S., Xie S., Tacconi L., Knezek P., Vicuso P., Tacconi-Gorman L., Scoville N., Schneider S. 1995, ApJS 98, 219